A satellite observation-based analysis of cirrus ice crystal number concentrations and underlying cirrus formation mechanisms

删除[凯']: **A satellite observation-based analysis of the distribution and formation mechanism of ice crystal number concentration over the Tibetan Plateau**

Kai Wang[1], Xiaocong Wang[2], Qianshan He[3], Hong Nie[4], Yanyu Wang[5], and Yonghang Chen[6]

[1]College of Atmospheric Science, Nanjing University of Information Science and Technology, Nanjing, China

[2]Institute of Atmospheric Physics, Chinese Academy of Sciences, Beijing, China

[3]Shanghai Meteorological Bureau, Shanghai, China

[4]Qinghai Meteorological Service Centre, Xining, China

[5]State Environmental Protection Key Laboratory of Formation and Prevention of Urban Air Pollution Complex, Shanghai Academy of Environmental Sciences, Shanghai, China

[6]College of Environmental Science and Engineering, Donghua University, Shanghai, China

Correspondence to: Qianshan He (oxeye75@163.com)

删除[蛋挞]: Institute of Desert Meteorology, China Meteorological Administration, Urumqi,

设置格式[蛋挞]: 字体: （默认）Times New Roman, （中文）宋体, 小四, 字体颜色: 自动设置, 字距调整: 0 磅

Abstract.

Cirrus clouds typically form in the upper troposphere and play an important role in the Earth's energy balance and the atmospheric water cycle. This study utilizes DARDAR-Nice data within June to August from 2006 to 2016 (except 2011), combined with CloudSat cloud products and other related aerosol products, to analyze the distribution characteristics and some possible formation mechanisms of ice crystal number concentration (N_i) in cirrus clouds over the Tibetan Plateau (TP). The results indicate that Ni over the northern TP is generally lower than that over the southern TP. This contrast shows a certain connection with differences in aerosol occurrence and the intensity of convective activity between the two regions. The vertical distribution of N_i over the TP exhibits a characteristic V-shaped structure, which is dominated by homogeneous freezing. When deep convective activity occurs, N_i tends to increase at

删除[凯']: are located at the upper middle-lower troposphere

设置格式[凯']: 字体: （默认）Times New Roman, （中文）宋体, 小四, 字体颜色: 自动设置

设置格式[凯']: 字体: （默认）Times New Roman, （中文）宋体, 小四, 字体颜色: 自动设置

设置格式[凯']: 字体: （默认）Times New Roman, （中文）宋体, 小四, 字体颜色: 自动设置

the same altitude compared to non-convective conditions. In contrast, under dust- and smoke-influenced conditions, N_i is generally lower, which may be related to ice formation via heterogeneous nucleation. In addition, weak vertical motion near 400 hPa over the northern TP is linked to an earlier appearance of the N_i peak at altitudes below the homogeneous freezing threshold temperature (−38 ° C).

1 Introduction

Cloud is the key link in the energy and water vapor balance of the earth-atmosphere system and plays an important role in global weather and climate change (Wang and Zhao, 1994; Stephens, 2005). Cirrus clouds are composed of a large number of non-spherical ice crystal particles with a wide range coverage of Earth surface (Guignard et al., 2011; Baran, 2012), which can reflect solar short-wave radiation and absorb terrestrial long-wave radiation, affect the energy balance of the upper troposphere and stratosphere and play an important role in the global water cycle and climate change (Kienast-Sjögren et al., 2016). A definite knowledge of cirrus microphysical properties and their formation mechanism is an important prerequisite for deepening the understanding of global climate change.

The Tibetan Plateau (TP) is a highest and largest plateau of the world, known as the 'roof of the world', affects significantly the climate patterns in eastern and southwestern China, and even global, as well as the global water circulation system, due to the unique dynamic and thermal effects. In summer, South Asian high controls the TP, where the cirrus clouds show different characteristics from that in other regions along the same latitude. On the one hand, the TP and its southern slope serves as an important windows for troposphere-stratosphere material exchange, where the frequent deep convective activities in summer have transported water vapor and anthropogenic aerosol pollutants to the upper troposphere-lower stratosphere (UTLS) (Fu et al., 2006; Randel et al., 2010; Chen et al., 2019). On the other hand, the substantial elevation difference over the southern part of the TP and the topographic uplift movement promote warm and humid airmass rising into the upper troposphere, which is conducive to the occurrence and development of cirrus clouds (Zhao et al., 2019; Yang et al., 2020). Also, the accumulation of aerosols is conducive to the formation of cirrus ice crystals by heterogeneous nucleation.

设置格式[凯']: 字体: （默认）Times New Roman, （中文）宋体, 小四, 字体颜色: 自动设置

设置格式[凯']: 字体: （默认）Times New Roman, （中文）宋体, 小四, 字体颜色: 自动设置

删除[凯']: The results indicate that N_i over the northern TP is significantly lower than that over the southern region, mainly due to differences in underlying aerosol concentration and the intensity of convective activity. Dominated by homogeneous nucleation, N_i exhibits a typical 'V' shaped vertical profile over the TP. When deep convective activity occurs, it facilitates the increase in N_i. In contrast, dust and smoke aerosols hinder the formation of N_i through heterogeneous nucleation.. Additionally, the vertical wind velocity near 400 hPa in the northern TP approaches zero, causing the N_i peak to appear prematurely below the homogeneous nucleation threshold temperature (-38 ° C).

设置格式[凯']: 字体: （中文）宋体

设置格式[凯']: 字体: （中文）宋体

设置格式[凯']: 字体: （中文）宋体

设置格式[凯']: 字体: （中文）宋体

设置格式[凯']: 字体: （中文）宋体

设置格式[凯']: 字体: （中文）宋体

设置格式[凯']: 字体: （中文）宋体

删除[凯']: Baran, 2012; Guignard et al., 2011

删除[凯']: Chen et al., 2019; Fu et al., 2006; Randel et al., 2010

So far, the study on cirrus clouds over the TP mainly focused on the spatiotemporal variation characteristics, cloud height, and cirrus cloud formation mechanism. Xue et al. (2018) found that the occurrence frequence, average effective radius of ice particles and cloud top height reached the maximum in summer over the TP using Moderate-Resolution Imaging Spectroradiometer (MODIS). Gao et al. (2003) found that the occurrence frequency of cirrus clouds reached a maximum in April and a minimum in November by MODIS data. Chen and Liu (2005) found that the occurrence of cirrus clouds over the TP in March and April was closely related to the slow uplift of warm and humid airmass to the tropopause due to topographic effect. Li et al. (2005) found that deep convection activities affected by Asian Summer Monsoon (ASM) were closely related to cirrus cloud formation over the TP using satellite observations. Zhang et al. (2020) used Cloud-Aerosol Lidar and Infrared Pathfinder Satellite Observations (CALIPSO) to investigate the generation mechanism of plateau cirrus clouds, revealing that large-scale orographic uplift, temperature fluctuations, and deep convection play crucial roles in their formation.

Previous studies have shown that the formation of cirrus ice crystals is primarily governed by three mechanisms: deep convective cloud anvil overflow (Prabhakara et al., 1993; Wang et al., 1996), homogeneous nucleation and heterogeneous nucleation (wang et al., 1997; Chen et al., 2000; Cantrell and Heymsfield, 2005). Updrafts and strong horizontal currents in the upper troposphere induced by deep convective activities lead to rapidly spreading around into cloud anvils composed of ice crystal particles (Takahashi and Luo, 2012). The homogeneous freezing of supercooled water droplets or aqueous aerosol particles to form ice crystals requires temperatures below approximately −38 ℃ and sufficiently high ice supersaturation (Duft and Leisner, 2004; Murray et al., 2010). While heterogeneous nucleation to form ice crystals requires relatively higher ambient temperature but insoluble aerosol particles (such as black carbon, dust) as ice-nucleating particles (INPs) (Morris et al., 2004; Murray et al., 2010; Shi et al., 2015; Fan et al., 2019).

删除[凯']: Documented research suggests that the formation of cirrus ice crystal particles is at the mercy of three mainstream mechanisms

删除[凯']: Cantrell and Heymsfield, 2005;

删除[凯']: The homogeneous nucleation of water vapor to form ice crystals requires a temperature below -38℃ and high relative humidity.

删除[凯']: Fan et al., 2019;

Different formation mechanisms result in different effects on the microphysical characteristics of cirrus ice crystals, in which ice crystal number concentration (N_i)

plays a crucial role in understanding and characterizing cirrus clouds (Comstock et al., 2008). N_i is widely used as a key variable in cloud forecasting to predict cloud evolution and is potentially closely linked to aerosol concentrations, making it an important indicator for studying the impact of aerosols on ice cloud formation (Khain et al., 2000; Kay and Wood, 2008; Hendricks et al., 2011). However, current climate models and satellite observations face significant limitations in obtaining and utilizing N_i, which can lead to substantial biases in simulating cloud microphysical processes, evaluating aerosol-cloud interactions, and calculating indirect radiative effects (Zhang et al., 2013; Sourdeval et al., 2018). It is generally recognized that homogeneous nucleation is the dominant mechanism determining N_i (Cantrell and Heymsfield, 2005). When enough INPs occurs in the atmosphere, heterogeneous nucleation precedes homogeneous nucleation to form ice crystals, resulting in a consumption of a large amount of water vapor and a decrease in the ambient supersaturation. Suppressed homogeneous nucleation will further impede the increase in the N_i (Chen et al., 2000; Kärcher and Lohmann, 2003; Shi et al., 2017). In the region of less convective activities, the effective radius of ice particles increases with the increase of INPs. Jin et al. (2007) used a three-dimensional storm cloud model (IAP-CSM3D) to analyze the relation between convective activity and cirrus cloud, found that the number concentration of ice crystal formed by deep convective cloud anvil overflow decreases with a decrease in water vapor from the convective activity transports.

删除[凯']: supposed

删除[凯']: a

删除[凯']: to decide

However, the 3D-distribution characteristics of N_i and the corresponding contribution from deep convective cloud anvil overflow, homogeneous nucleation and heterogeneous nucleation over the TP is not very clear. This study uses liDAR-raDAR-Number concentration of ICE particles (DARDAR-Nice) data to analyze the spatial distribution characteristics of medium-upper cirrus clouds in summer from 2006 to 2016 (except 2011), over the TP. The formation mechanism of ice particles also be explored in combination of CALIPSO satellite aerosol products with reanalysis data. Furthermore, this also sheds light on the role of aerosols in the upper atmosphere of the TP in the process of cirrus ice crystal formation. The results

will contribute to a deeper understanding of the thermodynamic effects of the TP and further improve the accuracy of climate simulations.

2 Data and methods

2.1 Satellite observations

This study uses ten summers (June-July-August, JJA) of multi-satellite observations during 2006 to 2016, except for 2011 due to data gaps, to investigate the distribution characteristics and formation mechanism of ice crystal particles over the TP. The primary dataset is the DARDAR-Nice product, complemented by additional retrievals from CloudSat and CALIPSO observations.

The DARDAR-Nice PRO product provides high-vertical-resolution estimates of N_i retrieved along the A-Train satellite track. The retrievals are based on the VarCloud algorithm (Delanoë and Hogan, 2008; 2010), which combines observations from the Cloud Profiling Radar onboard CloudSat and the cloud-aerosol Lidar with Orthogonal Polarization (CALIOP) lidar on CALIPSO. DARDAR-Nice profiles are provided with a vertical resolution of 60 m. The product includes N_i values and corresponding uncertainty estimates for particle with size larger than 5, 25 and 100 μm. In this study, the standard error of N_i is derived directly from the icnc_5um_error variable, ensuring that the uncertainty associated with each profile is properly represented in the analysis. This production has been systematically and comprehensively evaluated based on theoretical considerations and a large body of in situ observations (Sourdeval et al., 2018). However, it tends to overestimate ice crystal number concentrations in cloud parcels warmer than -30 ° C, due to the assumption of a monomodal particle size distribution in the retrieval algorithm. To ensure the reliability of the results, this study focuses exclusively on clouds with temperatures below -30°C and discusses the N_i of ice crystals with sizes larger than 5 μm.

In addition, although ice water content (IWC) is also provided in the DARDAR-Nice product, it has not been specifically validated. Therefore, this study uses IWC data from the CloudSat 2B-CWC-RO product (ftp://ftp.cloudsat.cira.colostate.edu/), for which the retrieval quality and accuracy

have been discussed in detail by Austin et al. (2007, 2009). Besides 2B-CWC-RO, the CloudSat 2B-CLDCLASS-LIDAR product is employed, which classifies clouds into eight types across ten vertical layers with a horizontal resolution of 2.5 km × 1.4 km. Its classification algorithm integrates vertical and horizontal cloud structures, precipitation features, cloud temperature, and MODIS radiative measurements to enhance classification accuracy. These CloudSat products provide critical microphysical parameters and cloud classification necessary for understanding ice cloud properties.

CALIPSO can monitor the vertical distribution characteristics of clouds and aerosols, automatically identify aerosol types, and provide global aerosol horizontal distribution characteristics and vertical distribution information (Zheng et al., 2018). Liu et al. (2008) also conducted aerosol detection using CALIPSO, further confirming its effective aerosol detection capabilities.

Dust aerosols exhibit strong ice-nucleating activity and represent an important global source of INPs (Hoose and Möhler, 2012; Murray et al., 2012; Ladino Moreno et al., 2013). Meanwhile, sampling studies during biomass burning conducted by Prenni et al. (2012) and McCluskey et al. (2014) indicate that particles from biomass combustion constitute a significant regional source of INPs, particularly when other effective INPs are scarce. In addition, recent observational analyses by Mamouri et al. (2023) and Ansmann et al. (2025) suggest that smoke aerosols can exert a substantial influence on ice crystal formation at altitudes while temperatures fall below −30 °C. Therefore, this study primarily focuses on the role of dust and smoke aerosols. This study employs information from the Level-2 Version 5 kmCLay standard products of the CALIPSO satellite data spanning from 2006 to 2016 (except 2011) to assess the impact of dust and smoke aerosols on the formation of cirrus clouds.

In this study, both daytime and nighttime satellite observations are included, the aerosol information is used to characterize climatological, grid-cell-averaged aerosol occurrence rather than instantaneous cloud-aerosol collocation.

2.2 Reanalysis Data

To investigate atmospheric context for the satellite observations, this study

utilizes ERA5 reanalysis data from the European Centre for Medium-Range Weather Forecasts (ECMWF). ERA5 provides hourly global data at a spatial resolution of 0.25° × 0.25° across 37 vertical pressure levels, covering the period from 1979 to the present (Xie et al., 2021). The key variables used in this study are specific humidity and vertical wind velocity from ERA5, as well as temperature from satellite observations. Together, these three variables are essential for analyzing atmospheric conditions related to cirrus cloud formation and deep convective vertical transport.

Table 1. Overview of the satellite datasets and data products used in this study

Source	Dataset	Variable	Duration
DARDAR	DARDAR-Nice PRO	icnc_5um icnc_5um_error temperature	
Cloudsat	2B-CWC-RO	ice water content	2006 - 2016
	2B-CLDCLASS-LIDAR	Cloud type(deep convection)	(except 2011)
Calipso	Level-2 Version 5 kmCLay	Aerosol type(dust 、 smoke 、 clean)	
ERA5	Reanalysis	specific humidity vertical wind velocity	

2.3 Research Methods

The focus area of this study is the TP and its surrounding regions, spanning from 66°E to 106°E and 24°N to 40°N. The original orbital data of the DARDAR-Nice PRO product, 2B-CLDCLASS-LIDAR classification product and 2B-CWC-RO cloud product are interpolated into grid point data with a resolution of 2° × 2° based on the method outlined in Wang et al. (2023). The 2B-CLDCLASS-LIDAR deep convective cloud product was used to quantify deep convection. For each grid cell and time interval, the presence of one or more deep convective clouds was counted as a single

删除[凯']: , which are essential
设置格式[凯']: 默认段落字体, 字体: （默认）Times N
设置格式[凯']: 居中, 缩进: 首行缩进: 0 字符, 制表位
设置格式[凯']: 字体: （默认）Times New Roman, （中
设置格式[凯']: 字体: （中文）Times New Roman, 五号
设置格式[蛋挞]: 字体: （默认）Times New Roman, （中
设置格式[蛋挞]: 段落间距段前: 0 磅, 段后: 0 磅, 行距
带格式表格[蛋挞]
设置格式[蛋挞]: 字体: （默认）Times New Roman, （中
设置格式[凯']: 字体: 五号, 非倾斜
设置格式[凯']: 两端对齐, 段落间距段前: 0 磅, 段后: (
设置格式[凯']: 字体: （默认）Times New Roman, （中
设置格式[凯']: 段落间距段前: 0 磅, 段后: 0 磅, 行距:
设置格式[凯']: 两端对齐, 段落间距段前: 0 磅, 段后: (
设置格式[凯']: 字体: （默认）Times New Roman, （中
设置格式[凯']: 两端对齐, 段落间距段前: 0 磅, 段后: (
设置格式[凯']: 字体: （默认）Times New Roman, （中
设置格式[凯']: 字体: （默认）Times New Roman, （中
设置格式[凯']: 字体: （默认）Times New Roman, （中
设置格式[凯']: 两端对齐, 段落间距段前: 0 磅, 段后: (
设置格式[凯']: 字体: （默认）Times New Roman, （中
设置格式[凯']: 字体: （默认）Times New Roman, （中
设置格式[凯']: 两端对齐, 段落间距段前: 0 磅, 段后: (
设置格式[凯']: 缩进: 首行缩进: 0 字符

event, irrespective of the number of profiles exhibiting convection. These events were then summed over all intervals to yield the total number of deep convection occurrences per grid cell. For the investigation of N_i, statistical analysis was conducted at intervals of 60 m, based on the vertical resolution of the DARDAR-Nice PRO product. Data points with large uncertainties were set to NaN to minimize bias in the statistics.

The horizontal distribution of N_i may be influenced by uneven sample distribution resulting from the varying occurrence frequency of ice particles across different layers. To address this, we normalized N_i for each grid during the ten summer seasons over the TP, to obtain the horizontal distribution of N_i for cirrus clouds. The normalization process is presented in Eq. (1):

$$y = \frac{\sum_{i=1}^{Num} x_i}{\sum_{i=1}^{Num} m_i} \quad (1)$$

Where x_i is the sum of N_i where the temperature is below -30°C. Num is the total number of profiles included in the analysis, m_i is the effective layers within the corresponding grid cell for which N_i is greater than 0. y is the normalized N_i in the corresponding gird.

To compute the vertical distribution of N_i, each profile is analyzed layer by layer. For each profile, if N_i is present in any layer, the profile is counted as 1; this count is used for normalizing the total number of profiles. For each layer, the N_i from all profiles are summed and then divided by the total number of counted profiles, yielding the normalized N_i for that layer. The detailed calculation method is given in Eq. (2):

$$\overline{a_n} = \frac{\sum_{i=1}^{Num} a_{i,n}}{\sum_{i=1}^{Num} C_i} \quad (2)$$

设置格式[凯']: 两端对齐

$$y = \frac{\sum_{i=1}^{Num} x_i}{Num1}$$

删除[凯']: (1)

删除[凯']: n

删除[凯']:

删除[凯']: is the number of occurrences in the corresponding gird during the study period

设置格式[凯']: 字体: （默认）Times New Roman, （中文）Times New Roman, 小四, 字体颜色: 自动设置, 非突出显示

设置格式[凯']: 字体: （默认）Times New Roman, （中文）Times New Roman, 小四, 字体颜色: 自动设置, 非突出显示

where $\overline{a_n}$ represents the normalized N_i for layer n, $a_{i,n}$ is the N_i in layer n of profile i, C_i is the profile count ($C_i = 1$ if N_i is present in at least one layer of profile i, and $C_i = 0$ otherwise).

$$P_n = \frac{\sum_{i=1}^{Num} a_{i,n}}{\sum_{i=1}^{Num} C_i} \quad (2)$$

In the absence of INPs in the atmosphere, ice crystal formation occurs primarily through homogeneous nucleation. It is generally acknowledged that temperatures near −38 °C represent the threshold for homogeneous freezing of supercooled water droplets and aqueous aerosol particles under sufficiently high ice supersaturation (Duft and Leisner, 2004; Murray et al., 2010; Koop and Murray, 2016). Traditionally, the identification of homogeneous nucleation has relied primarily on temperature thresholds. However, due to the continuous dynamic growth of ice particles through condensation, accurate simulation remains challenging. Moreover, classical nucleation theory suggests that ice formation under purely homogeneous freezing conditions is generally considered to be uncommon in the natural atmosphere (Maeda, 2021).

A novel approach is proposed to identify homogeneous nucleation by leveraging aerosol classification data from the CALIPSO satellite over the TP during the summer from 2006 to 2016. Specifically, when aerosol types are classified as ‘clean’, it indicates a low concentration of INPs, favoring the dominance of homogeneous nucleation in ice crystal formation. Kim et al. (2018) performed a statistical analysis of different aerosol types in this product and found that ‘clean’ aerosols account for only about 1% of occurrences, representing background aerosol with very low concentration, which further supports the validity of this assumption. Grid points identified exclusively with ‘clean’ aerosol conditions are therefore considered to have undergone only homogeneous nucleation.

Although CALIPSO provides detailed vertical profiles of aerosols, this study does not explicitly use the height-resolved information. Instead, the aerosol occurrence is analyzed at the grid-cell level without distinguishing altitude. This approach is adopted for two main reasons. First, CALIPSO’s aerosol detection is most reliable in the lower troposphere, while its sensitivity decreases significantly at higher

删除[凯']: (2)

删除[凯']: P_j

删除[凯']: j

删除[凯']: N_{total} is the total number of profiles included in the analysis,

删除[凯']: x

设置格式[凯']: 下标

删除[凯']: $_{i,j}$

删除[凯']: j

删除[凯']: the

删除[凯']: of water vapor.

删除[凯']: It is generally acknowledged that -38°C represents the threshold for homogeneous ice nucleation of water vapor (Koop and Murray, 2016)

删除[凯']: purely homogeneous nucleation events are extremely rare in the natural atmosphere.

删除[凯']: Although CALIPSO has limitations in detecting aerosols in the upper troposphere due to sparse aerosol layers and weak signal strength (Mao et al., 2022), resulting in some micro-scale undetected aerosols may introduce small deviations in individual values,

设置格式[凯']: 字体: （默认）Times New Roman, （中文）宋体, 字体颜色: 自动设置, 字距调整: 1 磅, （复杂文种）阿拉伯语(沙特阿拉伯)

设置格式[凯']: 字体: （默认）Times New Roman, （中文）宋体, 字体颜色: 自动设置, 字距调整: 1 磅, （复杂文种）阿拉伯语(沙特阿拉伯)

设置格式[凯']: 字体: （默认）Times New Roman, （中文）宋体, 字体颜色: 自动设置, 字距调整: 1 磅, （复杂文种）阿拉伯语(沙特阿拉伯)

altitudes due to signal attenuation and the difficulty of distinguishing aerosols from thin cirrus clouds (Mao et al., 2022). Therefore, focusing on overall aerosol occurrence within each grid ensures better data consistency and avoids potential misclassification errors. Second, the N_i analyzed in this study corresponds to temperatures below -30 ℃, the relevant aerosols are those that can influence cloud formation through vertical transport or large-scale dynamical processes, rather than being co-located at the same altitude. Hence, by integrating aerosol occurrence over the entire column within the same grid, the analysis effectively captures the overall influence of low-level dust or smoke aerosols on upper-tropospheric ice clouds, without introducing additional uncertainty from vertical matching. Therfore, the overall comparison, statistical results, and main conclusions remain robust.

3 Results and Discussion

3.1 Distribution characteristics of *N*N_i over the TP

Based on the DARDAR-Nice PRO product, this study analyzes the spatial variation of N_i across all layers where the temperature is below -30°C during the study period. The horizontal distribution of N_i in Fig. 1 demonstrates that the average concentration over the TP is 187 L^{-1} during the study period. This value is higher than the approximately 150 L^{-1} over the TP reported by Gryspeerdt et al. (2018), who used DARDAR-Nice data from 2006 to 2013 to study global N_i but focused only on cloud-top statistics. Considering that our analysis includes all layers below -30°C, the higher N_i is reasonable and consistent with physical expectations, which also indirectly supports the reliability of our results. The average concentration in the south (24-30°N, 66-106°E) is significantly higher than other areas, reaching 213 L^{-1}, with the maximum value located in the north-central region of India (24-26°N, 78-80°E), reaching 253 L^{-1}. Over the north, including the Xinjiang, Inner Mongolia, the north of the Qilian Mountains and the Kunlun Mountains, N_i is only 143 L^{-1}, only two-thirds of N_i compared with that in the southern region.

设置格式[凯']: 字体: （默认）Times New Roman, （中文）宋体, 字体颜色: 自动设置, 字距调整: 1 磅, （复杂文种）阿拉伯语(沙特阿拉伯)

设置格式[凯']: 字体: （默认）Times New Roman, （中文）宋体, 字体颜色: 自动设置, 字距调整: 1 磅, （复杂文种）阿拉伯语(沙特阿拉伯)

设置格式[凯']: 字体: （默认）Times New Roman, （中文）宋体, 字体颜色: 自动设置, 字距调整: 1 磅, （复杂文种）阿拉伯语(沙特阿拉伯)

设置格式[凯']: 字体: （默认）Times New Roman, （中文）宋体, 字体颜色: 自动设置, 字距调整: 1 磅, （复杂文种）阿拉伯语(沙特阿拉伯)

删除[凯']: this study focuses on large-scale ice crystal formation events over the TP during the ten summer seasons from 2006 to 2016 (except 2011), including both homogeneous and heterogeneous nucleation.

删除[凯']: .48

删除[蛋挞]: This value is

删除[凯']: comparable to the annual mean

设置格式[凯']: 字体: （默认）Times New Roman, （中文）宋体, 小四, 字体颜色: 自动设置

删除[凯']: and found values of around 150 L^{-1} over the TP.

删除[凯']: Furthermore, it falls within the range obtained from in-situ measurements of high-altitude summer cirrus clouds reported by Cairo et al. (2023), who observed N_i ranging from 0.1 to 10^4 L^{-1} over the Himalayas during July and August 2017, coinciding with the ASM. The agreement with the independent in-situ observations reinforces the reliability of our satellite-derived N_i estimates and indicates that the DARDAR-Nice product can effectively capture the microphysical properties of cirrus clouds in such extreme environments.

删除[凯']: .12

删除[凯']: 2.95

删除[凯']: 2.75

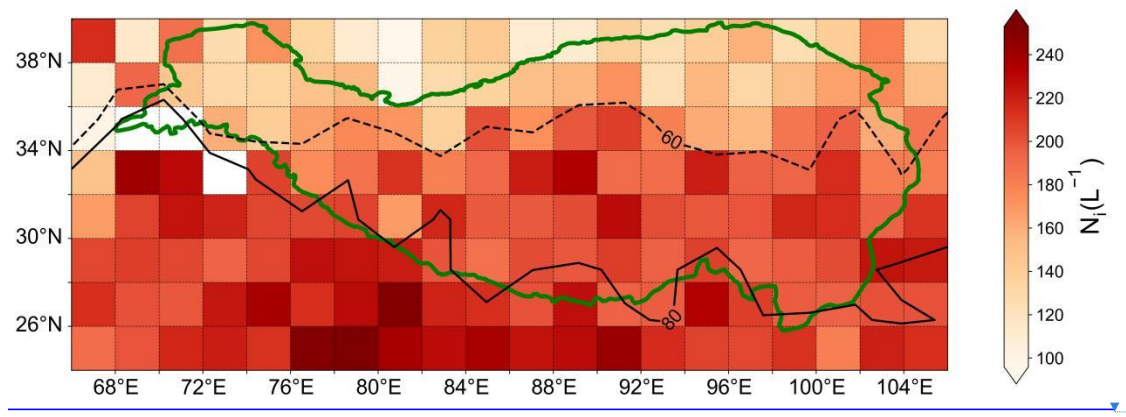

Fig. 1. Horizontal distribution of the averaged N_i during the summer from 2006 to 2016 (except 2011) over the TP. The green line is the border of the TP. The black solid lines represent the standard error of 80 L^{-1} and the black dotted line represents the value of 60 L^{-1}.

We investigated the relationship between the incidence of deep convective clouds, INPs, and N_i at all grid points over the TP based on the different formation mechanisms of cirrus clouds. As shown in Fig. 2a, deep convection occurrences (DCO) is significantly higher in the southern and southeastern regions of the Plateau, where the N_i tend to be elevated (Fig. 1). Also, N_i revealed a positive nonlinear relationship with DCO, with a coefficient of determination (R^2) of 0.55 ($p<0.01$) and a root mean square error (RMSE) of 24.03 L^{-1}, indicating that deep convective activity plays a significant role in modulating N_i over the TP. During the ASM, frequent deep convection in the southern TP facilitates the transport of warm, moist air and water droplets from the Indian Ocean and the Bay of Bengal to higher altitudes (He et al., 2019). Under moist conditions, ascending air parcels are more likely to experience a prolonged period of ice supersaturation, thereby increasing the probability of exceeding the supersaturation threshold required for homogeneous ice nucleation. In humid environments, air parcels can therefore maintain supersaturated conditions for a longer duration, making homogeneous nucleation more likely to dominate under such circumstances (Zhao et al., 2018). By contrast, heterogeneous nucleation is initiated by INPs and typically requires a lower ice supersaturation threshold, allowing it to occur earlier during ascent (DeMott et al., 2010). As a result, in environments with abundant water vapor, homogeneous nucleation may gain a

删除[凯']:

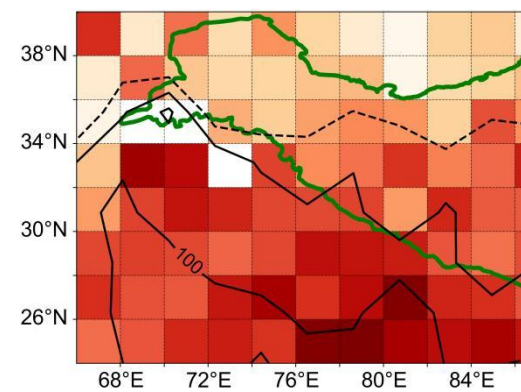

删除[凯']: and 100 L-1

设置格式[凯']: 非上标/ 下标

删除[凯']: .

删除[凯']: T

删除[凯']: （

设置格式[凯']: 字体: （中文）Times New Roman, 非突出显示

设置格式[凯']: 字体: （默认）Times New Roman, （中文）Times New Roman, 小四, 字体颜色: 自动设置

删除[凯']: water droplets）

设置格式[凯']: 字体: （中文）Times New Roman, 非突出显示

设置格式[凯']: 字体: （中文）Times New Roman

relative advantage in competition with heterogeneous nucleation, favouring the formation of higher N_i.

This interpretation is consistent with the relatively high N_i observed over the southern TP during summer. However, within an observational framework alone, the respective contributions of dynamical conditions, aerosol properties, and thermodynamic processes cannot be fully disentangled. The interpretation presented here should therefore be regarded as a qualitative explanation based on physical consistency rather than a definitive attribution.

In addition to convective activity, the presence of INPs also plays a critical role in modulating N_i over the TP. Zhao et al. (2018), using nine years of satellite observations, demonstrated that ice crystal formation is regulated not only by the availability of INPs but also by ambient water vapor conditions. This highlights the important role of moisture as a prerequisite for cirrus cloud evolution, while emphasizing that high water vapour availability alone is not sufficient to guarantee ice formation. Ice nucleation can only occur when the ice saturation ratio exceeds the threshold required for freezing; without reaching this threshold, no ice formation is possible (Gettelman et al., 2010). As a result, moisture should be regarded as a necessary background condition rather than a direct or sufficient driver of ice crystal formation.

Consequently, when investigating the relationship between INPs and N_i, directly comparing INPs and N_i across all grid cells may lead to misleading interpretations. This is because differing atmospheric conditions, particularly variations in moisture and the development of ice supersaturation, can strongly influence whether ice formation occurs. For example, high N_i in one grid cell may primarily reflect favourable moisture conditions that allow supersaturation to be achieved, rather than an enhanced influence of INPs, whereas in another grid cell the potential effect of INPs may be masked if the supersaturation threshold is not exceeded.

In principle, restricting the analysis to grid cells with broadly similar atmospheric conditions would allow a more direct comparison. However, the TP exhibits pronounced spatial heterogeneity, especially between its northern and southern

regions. To partially account for differences in moisture-related thermodynamic conditions, this study introduces the IWC confined INPs concentration (ICIC), defined as the logarithm of the ratio between the occurrence number of smoke (or dust) particles and IWC within each grid cell (Eq. 3). By standardization, this metric improves the comparability of the analysis to some extent. To further demonstrate the robustness of this normalization, we compute the partial correlation between INPs and N_i after removing the effect of IWC. The resulting coefficient, r = -0.38, confirms that the ICIC formulation effectively reduces moisture-related confounding.

$$ICIC\ (type) = log\ (\frac{type_{event}}{IWC}) \quad (3)$$

Where *type* is dust or smoke, $type_{event}$ is the number of events of that aerosol type, and *ICIC(type)* is the ICIC value corresponding to that aerosol type in the corresponding gird.

Fig.3a shows the spatial distribution of this metric, revealing that ICIC is predominantly concentrated in the northern part of the Plateau, with significantly lower values in the south. Moreover, an inverse nonlinear relationship is observed between ICIC and N_i, with a coefficient of determination (R^2) of 0.61 ($p<0.01$) and a root mean square error (RMSE) of 22 L^{-1}, indicates that the quantity of ICIC has a significant impact on the N_i over the TP. While the N_i mainly arises from homogenization nucleation, heterogeneous nucleation of INPs promotes the formation of ice crystals (Khvorostyanov et al., 2006; DeMott et al., 2010) by absorbing a large amount of water vapor and destroying the conditions for homogeneous nucleation. The inhibitory effect of heterogeneous nucleation on homogeneous nucleation becomes more pronounced with an increase in INPs content, leading to a lower N_i. These two factors, namely the increased convective cloud frequency in the south and the elevated INPs levels in the north, are the primary contributors to the observed spatial pattern of N_i, which tends to be higher in the south and lower in the north.

删除[凯']: This highlights the crucial role of moisture in modulating cirrus formation pathways and underscores the need to account for water vapor when assessing the influence of INPs. Therefore, when investigating the relationship between INPs and N_i, directly comparing INPs and N_i acro

设置格式[凯']: 字体: （默认）Times New Roman, （中文）宋体, 小四, 字体颜色: 自动设置

设置格式[凯']: 字体: （默认）Times New Roman, （中文）宋体, 小四, 字体颜色: 自动设置

设置格式[凯']: 字体: （默认）Times New Roman, （中文）宋体, 小四, 字体颜色: 自动设置

设置格式[凯']: 字体: （默认）Times New Roman, （中文）宋体, 小四, 字体颜色: 自动设置

设置格式[凯']: 字体: （默认）Times New Roman, （中文）宋体, 小四, 字体颜色: 自动设置

设置格式[凯']: 字体: 倾斜

设置格式[凯']: 字体: 倾斜

设置格式[凯']: 字体: （默认）Times New Roman, （中文）宋体, 小四, 字体颜色: 自动设置

设置格式[凯']: 字体: （默认）Times New Roman, （中文）宋体, 小四, 字体颜色: 自动设置

设置格式[凯']: 字体: 倾斜

设置格式[凯']: 字体: （默认）Times New Roman, （中文）宋体, 小四, 字体颜色: 自动设置

设置格式[凯']: 字体: （默认）Times New Roman, （中文）宋体, 小四, 字体颜色: 自动设置

删除[凯']: 1.94

删除[凯']: larger

删除[凯']: DeMott et al., 2010;

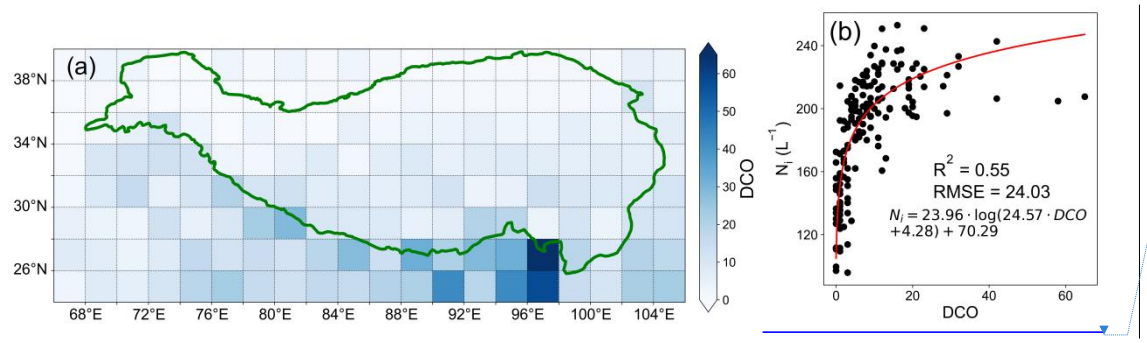

Fig. 2. (a) Horizontal distribution of DCO and **(b)** the relationship with N_i during the summer from 2006 to 2016 (except 2011) over the TP.

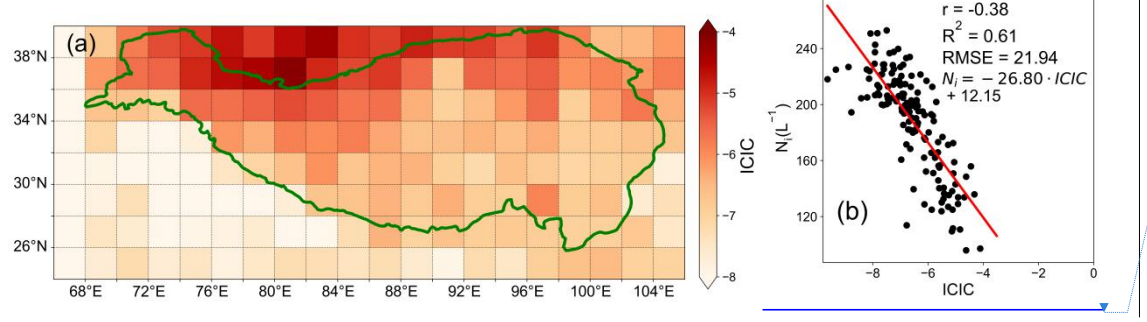

Fig. 3. (a) Horizontal distribution of the ICIC and **(b)** the relationship with N_i during the summer from 2006 to 2016 (except 2011) over the TP. r(-0.38) in this figure is the partial correlation coefficient between INPs and Ni after removing the effect of IWC.

3.2 Generation mechanism of ice crystal formation

3.2.1 Contribution of the homogeneous nucleation

Due to the condensation growth of cirrus cloud ice crystals in the upper atmosphere after nucleation, the observed ice crystal particle size in the satellite observation dataset only represents the post-growth effect, rendering it impossible to distinguish the contribution of different nucleation mechanisms to ice crystal size. Thus, this study considered the contribution of different nucleation mechanisms to the formation of cirrus cloud ice crystals by examining changes in the N_i.

N_i for each vertical layer is calculated using Eq. (2), and Fig. 4 depicts the vertical distribution of the N_i from satellite observations and homogeneous nucleation. In cases where CALIOP does not indicate the presence of dust or smoke and the aerosol type is classified as 'clean', ice formation is assumed to occur via homogeneous freezing.

The satellite observations indicate that the N_i initially slowly increases with height and reaches its maximum of 68 L^{-1} at 14 km, and follows a decreasing trend with height up to 19 km. The vertical variation of N_i from homogeneous nucleation and observation both show an overall 'V' shaped distribution. However, N_i derived from homogeneous nucleation is consistently higher than the satellite observations at corresponding altitudes. Specifically, the number concentration from homogeneous nucleation peaks at 14 km with a value of 94 L^{-1}, which coincides with the altitude of the observed peak.

删除[凯']: 7.56

删除[凯']: .35

It is widely accepted that the formation of larger ice crystals through heterogeneous nucleation processes takes precedence over homogeneous nucleation (Shi et al., 2017; Barahona and Nenes, 2009). In fact, heterogeneous nucleation is the dominant ice formation mechanism at temperatures above -38 ℃ , whereas homogeneous nucleation occurs only when the temperature drops below -38℃ and when there are no INPs. Although homogeneous nucleation is the major contributor to the N_i (Cantrell and Heymsfield, 2005), heterogeneous nucleation has lower activation requirements and may occur earlier, potentially consuming water vapor and influencing subsequent ice formation. Under this interpretation, the observed N_i being lower than that expected under conditions favorable for homogeneous freezing could be consistent with the influence of heterogeneous nucleation. However, alternative explanations cannot be excluded. For example, lower N_i may also reflect weaker or less frequent updrafts, which would limit the development of high ice supersaturation, or differences in cloud origin, such as a predominance of in-situ cirrus with limited contribution from liquid-origin ice detrained from deep convective updrafts (Gryspeerdt et al., 2018; Lyu et al., 2025).

Additionally, it is also worth noting that the observed N_i slightly exceeds the values from homogeneous nucleation below approximately 12 km. This is likely because homogeneous nucleation has not yet become dominant in this layer, while the observed N_i reflects prior heterogeneous nucleation events that produced a relatively large number of ice crystals. Once homogeneous nucleation becomes active with decreasing temperature, it rapidly generates a substantially higher N_i than observed.

删除[凯']: heterogeneous nucleation has relatively low formation requirements and often occurs prior to homogeneous nucleation. During this process, a large amount of water vapor is absorbed, which further suppresses the formation of ice crystals through homogeneous nucleation. This mechanism also explains why the observed N_i is significantly lower than that produced only by homogeneous nucleation.

From a trend perspective, the 'V' shape vertical distribution and the peak position of N_i is determined by the role of homogeneous nucleation, while the specific values at different altitudes are determined by the combined effect of homogeneous nucleation and heterogeneous nucleation.

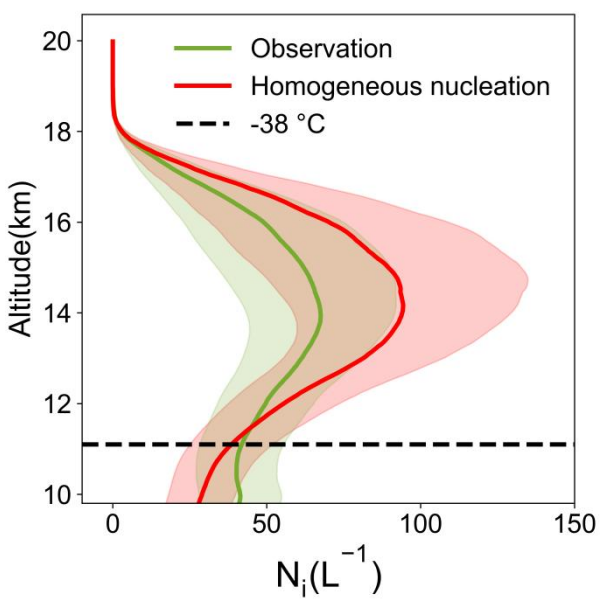

Fig. 4. Vertical profiles of observed and homogeneously nucleated N_i, with light shading indicating the standard error range.

To further investigate the vertical distribution characteristics of N_i, this study analyzes its spatial distribution across different latitudes and longitudes based on Fig. 5. In the zonal cross-section (Fig. 5a), the N_i exhibits a pronounced maximum near 14 km altitude between 28°N and 33°N, exceeding 120 L^{-1}. Additionally, in the meridional cross-section (Fig. 5b), a peak N_i of over 90 L^{-1} is observed near 90°E, also centered at 14 km altitude.

Together, these zonal and meridional distributions reveal a consistent vertical structure, with peak N_i occurring near 14 km, which could be influenced by homogeneous nucleation processes that dominate at these altitudes (Fig. 4). In contrast, N_i exhibits significant variability across both latitudinal and longitudinal directions, which may be related to the spatial distribution of water vapor and certain meteorological factors, such as vertical wind velocity, providing a foundation for the

删除[凯']: primarily driven by

删除[凯']:

subsequent analysis in this study.

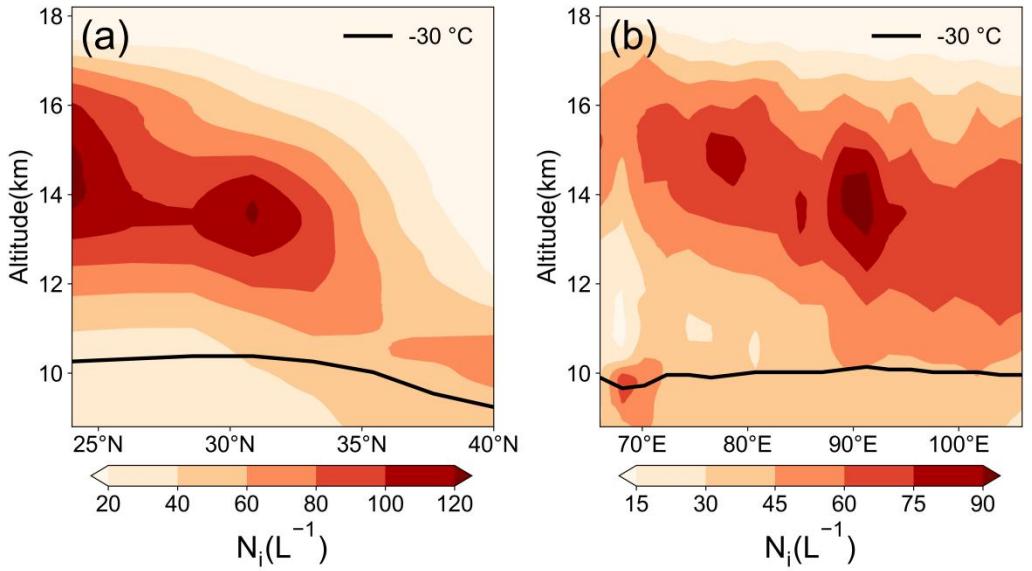

Fig. 5. (a) The zonal distribution of N_i from 86 to 102°E for each latitude and (b) the meridional distribution of N_i from 24 to 40°N for each longitude.

3.2.2 The effect of deep convective activity

In addition to homogeneous nucleation, deep convective cloud anvils are another significant source of ice crystal formation in the atmosphere. Fig. 6a compares the altitude-averaged N_i under different deep convective cloud conditions, based on all grid points across the TP where the incidence of deep convection exceeds 5% (Fig. 2a). These selected regions represent areas with relatively frequent convective activity.

During summer, the tropopause height over the Tibetan Plateau typically ranges from about 16 - 18 km (Sun et al., 2021), providing an important vertical reference for cirrus cloud development. The top of cirrus clouds can develop near 18 km with a relatively low N_i for the case of non-deep convection activity, and at 14 km, reaches its peak of 104 L^{-1}. When deep convection activity occurs, the N_i at the same altitude is significantly higher, and at 14 km, reaches its peak of 162 L^{-1}. During summer, strong upward motions over the southern TP can transport both moist air and pre-existing ice crystals from the lower troposphere (below 12 km) into the upper troposphere via convective outflow anvils. These processes may create favorable

删除[凯']: is likely influenced by the spatial heterogeneity of aerosol-derived INPs and the localized intensity of deep convection.

删除[凯']: 3.94

删除[凯']: 1.84

conditions for enhanced N_i, while homogeneous nucleation may additionally occur under sufficiently cold and supersaturated conditions. It is therefore suggested that the observed N_i peak near 14 km is associated with the combined effects of convective transport, dynamical accumulation, and ice formation processes. At 14 km (about 140 hPa), where the vertical wind speed is nearly zero, N_i accumulates significantly above this level, while a substantial amount is transported upward from below 14 km. This upward transport, combined with the accumulation, results in the peak at 14 km (Fig. 4b). Satellite observations also indicate that during the development of deep convective clouds, approximately 95% of the cloud tops are located at or below 16 km. This vertical distribution suggests that the influence of deep convection is mainly confined below 16 km. Consequently, N_i above this level remains relatively unchanged, indicating limited impact from convective processes at higher altitudes.

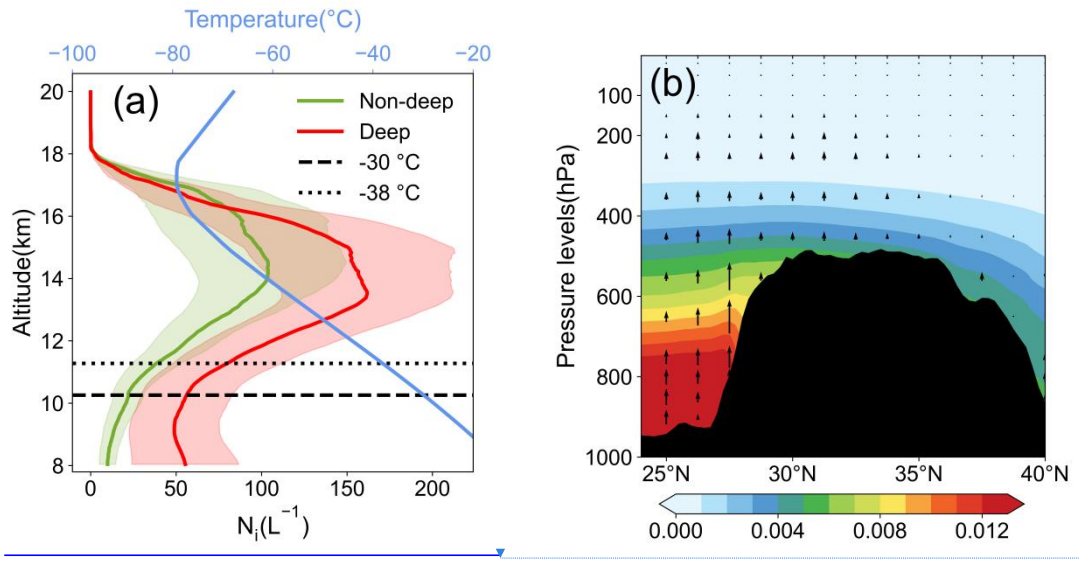

Fig. 6. (a) Vertical profile of the N_i affected by DCO and **(b)** the zonal distribution of vertical winds averaged from 86 to 102°E for each latitude. The contour is specific humidity (kg kg^{-1}).

3.2.3 Heterogeneous nucleation effect of INPs

In the northern part of the TP, convective activity is relatively weak, but dust aerosol content is high (Fig. 7a). The increase in N_i is primarily attributed to heterogeneous nucleation induced by INPs. Considering the frequent dust activity in

删除[凯']: In summer, strong upward motion over the southern TP transports a large amount of water vapor from the lower atmosphere to the upper atmosphere (Fig. 6b), resulting in a significant increase of Ni by the homogeneous nucleation process. It is evident that the Ni of cirrus clouds peaks at 14 km, which is due to deep convective activity.

设置格式[凯']: 字体: （中文）Times New Roman

设置格式[凯']: 字体: （中文）Times New Roman

设置格式[凯']: 字体: （中文）Times New Roman

设置格式[凯']: 字体: （中文）Times New Roman

设置格式[凯']: 字体: （中文）Times New Roman

设置格式[凯']: 字体: （中文）Times New Roman

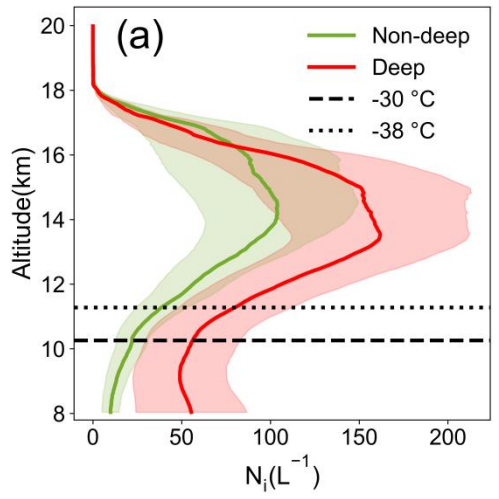

删除[凯']:

this region, we selected grid points with ICIC(dust) greater than -5 as the primary study area. These grid points are predominantly located in the northern Plateau, adjacent to Xinjiang, a typical semi-arid region characterized by abundant dust aerosols. These dust particles facilitate water vapor adsorption in the lower atmosphere and promote ice crystal formation through heterogeneous nucleation (Huang et al., 2021; Hoose and Möhler, 2012).

Fig. 7b illustrates the effect of dust aerosol particles on N_i in this area. The results suggest that the presence of dust is associated with a reduction of N_i in cirrus clouds, with concentrations above 12 km becoming very small. During non-dust periods, although INPs remain present, their activation efficiency may be relatively high, allowing a large fraction of aerosol ice nuclei to be activated, resulting in weaker suppression of ice crystal formation. In contrast, elevated dust concentrations in the lower atmosphere may enhance heterogeneous nucleation, thereby consuming available water vapor and potentially inhibiting additional ice crystal formation, which could lead to a reduction of N_i. Within this interpretative framework, N_i during non-dust periods tends to be higher than during dust conditions. However, due to limited water vapor in this region, a large fraction of moisture may already be depleted in the lower atmosphere, which could contribute to very low N_i above 12 km. Consequently, the suppressive effect of heterogeneous nucleation may limit ice crystal formation through homogeneous nucleation at higher altitudes, making cirrus cloud development more difficult in these upper layers. In regions with low water vapor content, INPs may play an important role in modulating N_i.

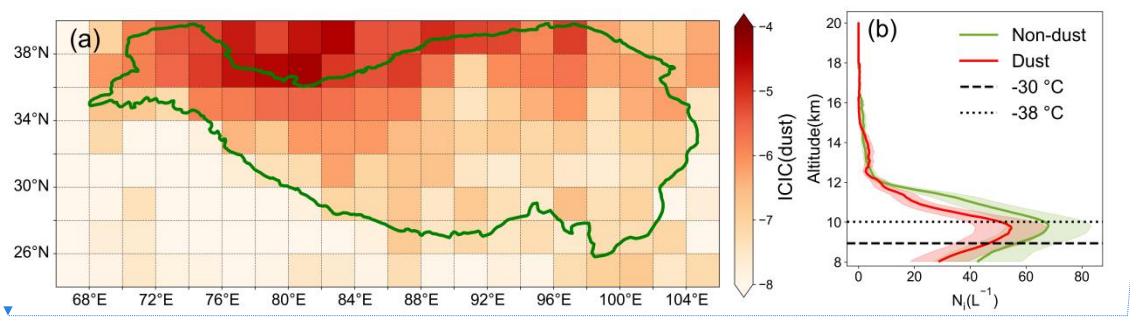

Fig. 7. (a) Horizontal distribution of ICIC(dust) and **(b)** the vertical profile of the N_i affected by dust and non-dust events.

删除[凯']: Fig. 7b illustrates the effect of dust aerosol particles on N_i in this area. The results indicate that the presence of dust significantly reduces N_i in cirrus clouds, with concentrations above 12 km nearly approaching zero. During non-dust periods, although INPs remain present, their activation efficiency is high, nearly all aerosol ice nuclei are activated to form ice crystals, resulting in relatively weak suppression among heterogeneous nucleation processes. In contrast, elevated dust concentrations in the lower atmosphere enhance heterogeneous nucleation, thereby consuming available water vapor and inhibiting additional ice crystal formation, which leads to a significant reduction of N_i. This explains why N_i during non-dust periods is higher than that during dust. However, due to limited water vapor in this region, most moisture is depleted in the lower atmosphere, causing N_i above 12 km to be nearly zero. Consequently, the suppressive effect of heterogeneous nucleation inhibits ice crystal formation through homogeneous nucleation at higher altitudes, making cirrus cloud development more difficult in these upper layers. Therefore, it can be concluded that in regions with low water vapor content, INPs plays a dominant role in determining N_i.

删除[凯']: aerosols

Besides dust aerosol, smoke aerosol particles generated by human activities are considered another potential source of heterogeneous nucleation for cirrus clouds over the TP. In this research, grid points with ICIC(smoke) greater than −6.5 were selected as the primary research region to examine the possible influence of smoke INPs on N_i (Fig. 8a).

It is observed that the presence of smoke aerosols is associated with a decrease in N_i, with the maximum vertical extent of cirrus clouds limited to around 14 km (Fig. 8b). One possible interpretation is that, during smoke events, ice crystal formation in the lower atmosphere may be influenced by smoke-derived INPs, under which heterogeneous nucleation could become more active. The relatively high abundance of smoke INPs may enhance competition among ice particles, potentially suppressing additional ice crystal formation and resulting in lower N_i compared to non-smoke conditions. In this hypothetical framework, smoke INPs may be efficiently activated through heterogeneous nucleation, while any remaining water vapor could still contribute to ice formation via homogeneous nucleation. From this perspective, N_i tends to be higher during non-smoke periods, when fewer INPs may lead to weaker suppression effects. However, due to the inherently low water vapor content in this region, the vertical development of cirrus clouds appears to be constrained, and even during non-smoke periods, the maximum cloud height remains limited to approximately 17 km.

Homogeneous nucleation is often associated with a peak in N_i near 14 km. However, under dust and smoke conditions, such a peak is not clearly observed. One possible explanation is that dust and smoke aerosols are mainly concentrated over the northern TP, where the vertical wind speed around 400 hPa is relatively weak (Fig. 6b). Reduced vertical transport may limit the upward redistribution of ice crystals, thereby influencing the vertical structure of N_i.

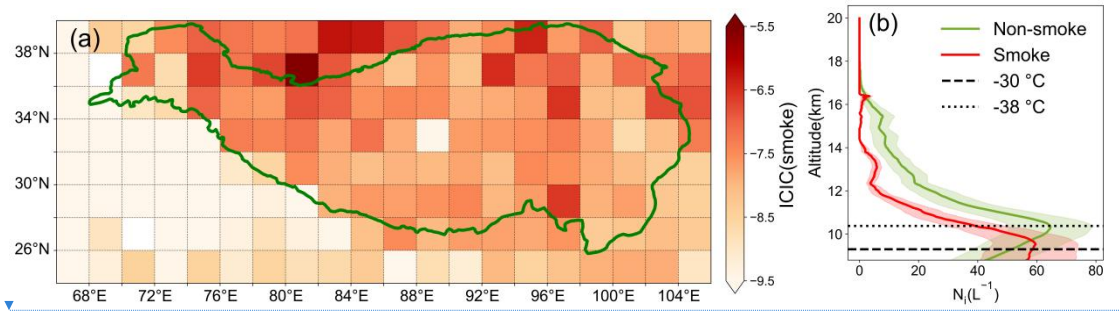

Fig. 8. (a) Horizontal distribution of ICIC(smoke) and **(b)** the vertical profile of the N_i affected by smoke and non-smoke events.

4 Conclusion

This study analyzed the distribution characteristics and formation mechanism of cirrus cloud ice crystals during the summer of 2006 to 2016 (except 2011) over the TP, mainly using DARDAR-Nice data combined with aerosol product data.

The main conclusions are summarized as follows: (1) N_i shows pronounced spatial variability across the TP, with generally higher values over the southern TP than over the northern TP. This contrast is statistically associated with differences in large-scale meteorological conditions, including more frequent deep convection over the southern TP, whereas the northern TP is characterized by more frequent aerosol occurrence and lower N_i.

(2) The vertical distribution of N_i exhibits a characteristic V-shaped structure, consistent with statistical signatures expected under conditions favorable for homogeneous freezing. The values of N_i at varying altitudes are likely determined by the combined effects of both homogeneous and heterogeneous nucleation.

(3) Regions influenced by deep convection tend to exhibit higher N_i at a given altitude than non-convective regions. This behavior is consistent with the role of convective outflow anvils in transporting moisture and pre-existing ice crystals into the upper troposphere, while homogeneous freezing may additionally occur under sufficiently cold and supersaturated conditions.

(4) Under dust and smoke influenced conditions, ice formation in the lower atmosphere is statistically associated with heterogeneous nucleation occurring prior to

删除[凯']: Besides dust aerosol, smoke aerosol particles generated by human activities are another important source of heterogeneous nucleation for cirrus clouds over the TP. In this research, grid points with ICIC(smoke) greater than -6.5 were selected as the primary research region to analyze the impact of smoke INPs on N_i (Fig. 8a).

It is observed that the presence of smoke aerosols leads to a decrease in N_i, with the maximum development height of cirrus clouds limited to around 14 km (Fig. 8b). During smoke events, ice crystal formation in the lower atmosphere is primarily governed by smoke-derived INPs, where heterogeneous nucleation dominates. The high abundance of smoke INPs causes strong competition among ice particles, suppressing additional ice crystal formation and resulting in a lower N_i compared to non-smoke events. During smoke events, the utilization efficiency of smoke INPs is nearly 100%, meaning that almost all available INPs are activated to form ice crystals through heterogeneous nucleation. Any excess water vapor not consumed by this process may still contribute to ice formation via homogeneous nucleation. This explains why N_i is generally higher during non-smoke events that fewer INPs lead to weaker suppression effects and more efficient homogeneous nucleation. However, due to the inherently low water vapor content in this region, the vertical development of cirrus clouds is constrained. Even during non-smoke events, the maximum height of cirrus clouds is limited to approximately 17 km.

Notably, homogeneous nucleation typically leads to a peak in N_i at 14 km. However, in cases involving dust and smoke aerosols, this peak is not observed. This is primarily because dust and smoke are concentrated in the northern TP, where the vertical wind speed at around 400 hPa is nearly zero (Fig. 6b). The weak vertical transport prevents ice crystals from being carried upward efficiently, resulting in their accumulation in the upper atmosphere. Therefore, the N_i peak appears near the homogeneous nucleation threshold temperature (−38°C), suppressing its development at around 14 km altitude.

删除[凯']: aerosols

homogeneous freezing, and N_i is generally lower than non-dust(smoke) conditions. This behavior may be related to early vapor consumption, differences in vertical motion, and sedimentation effects. These interpretations represent one possible explanation of the observed.

Several limitations should be noted. This study integrates several validated satellite retrieval products in the analysis. Nevertheless, differences in retrieval methodologies and sensor sensitivities among these products introduce inherent uncertainties, which may affect the quantitative interpretation of the results to some extent. In addition, the use of multi-year climatological averages smooths event-scale extremes associated with strong updrafts or short-lived dynamical processes. Aerosol information represents grid-cell-scale and climatological conditions rather than instantaneous cloud–aerosol interactions. Consequently, the results should be regarded as hypothesis-driven and exploratory, providing statistical context and motivation for future studies combining satellite observations, in-situ measurements, and modeling.

Acknowledgements. This study was supported by the National Natural Science Foundation of China (NSFC, Grant Numbers: 42330603), the Open Research of Key Laboratory of Intelligent Meteorological Observation Technology in China Meteorological Administration (ZNGC2024ZD02), the Science and Technology Planning Program of Xinjiang (2022E01047), National Natural Science Foundation of China (42030612 and 42175179), and the Natural Science Foundation of Shanghai (22ZR1404000). The authors gratefully acknowledge the ECMWF for providing ERA5 data, and the NASA for providing CloudSat and CALIPSO data. In addition, the DARDAR-Nice product used in this study was obtained from the AERIS/ICARE data center.

References

Ansmann, A., Jimenez, C., Knopf, D. A., Roschke, J., Bühl, J., Ohneiser, K., and Engelmann, R.: Impact of wildfire smoke on Arctic cirrus formation–Part 2: Simulation of MOSAiC 2019–2020 cases, Atmos. Chem. Phys., 25, 4867-4884, 2025.

Austin, R. T., Heymsfield, A. J., and Stephens, G. L.: Retrieval of ice cloud microphysical parameters using the CloudSat millimeter-wave radar and temperature, J. Geophys. Res., 114, doi:10.1029/2008JD010049, 2009.

Austin, R. T.: Level 2B radar-only cloud water content (2B-CWC-RO) process description document, Data Processing Center, 24, 2007.

Barahona, D. and Nenes, A.: Parameterizing the competition between homogeneous and heterogeneous freezing in

删除[凯']: The N_i show clear spatial differences across the TP. The N_i is significantly higher over the southern TP, where frequent deep convection promotes ice crystal formation, compared with the northern TP, where more abundant aerosols are present and N_i remains relatively low.
Homogeneous nucleation leads to a characteristic 'V' shaped distribution of N_i. The values of N_i at varying altitudes are determined by the combined effects of both homogeneous and heterogeneous nucleation.
Deep convection activities are found to promote the concentration of ice crystals. The deep convective cloud anvil enhances the N_i at the same altitude compared to non-deep convective activities.
The presence of dust and smoke aerosols leads to ice crystal formation via heterogeneous nucleation in the lower atmosphere, occurring before homogeneous nucleation. Heterogeneous nucleation suppresses further ice crystal formation, resulting in lower concentrations compared to non-dust and non-smoke conditions. Additionally, the vertical velocity at high altitudes drops to zero earlier, causing the ice crystal number concentration peak to appear prematurely.

设置格式[凯']: 无项目符号或编号

ice cloud formation-polydisperse ice nuclei, Atmos. Chem. Phys., 9, 5933-5948, 2009.

Baran, A. J.: From the single-scattering properties of ice crystals to climate prediction: A way forward, Atmos. Res., 112, 45-69, 2012.

Cairo, F., Krämer, M., Afchine, A., Di Donfrancesco, G., Di Liberto, L., Khaykin, S., Lucaferri, L., Mitev, V., Port, M., Rolf, C., Snels, M., Spelten, N., Weigel, R., and Borrmann, S.: A comparative analysis of in situ measurements of high-altitude cirrus in the tropics, Atmos. Meas. Tech., 16, 4899-4925, 2023.

Cantrell, W. and Heymsfield, A.: Production of ice in tropospheric clouds: A review, Bull. Am. Meteorol. Soc., 86, 795-808, 2005.

Chen, B. and Liu, X.: Seasonal migration of cirrus clouds over the Asian Monsoon regions and the Tibetan Plateau measured from MODIS/Terra, Geophys. Res. Lett., 32, doi:1029/2004GL020868, 2005.

Chen, Q. L., Gao, G. L., Li ,Y., Cai, H. K., Zhou, X., and Wang, Z. L.: Main detrainment height of deep convection systems over the Tibetan Plateau and its southern slope, Adv. Atmos. Sci., 36, 1078-1088, 2019.

Chen, Y., DeMott, P. J., Kreidenweis, S. M., Rogers, D. C., and Sherman, D. E.: Ice formation by sulfate and sulfuric acid aerosol particles under upper-tropospheric conditions, J. Atmos. Sci., 57, 3752-3766, 2000.

Comstock, J. M., Lin, R. F., Starr, D. O. C., and Yang, P.: Understanding ice supersaturation, particle growth, and number concentration in cirrus clouds, J. Geophys. Res. Atmos., 113, D23211, 2008.

Delanoë, J., and Hogan, R. J.: A variational scheme for retrieving ice cloud properties from combined radar, lidar, and infrared radiometer, J. Geophys. Res., 113, D07204, 2008.

Delanoë, J., and Hogan, R. J.: Combined CloudSat-CALIPSO-MODIS retrievals of the properties of ice clouds, J. Geophys. Res., 115, D00H29, 2010.

DeMott, P. J., Prenni, A. J., Liu, X., Kreidenweis, S. M., Petters, M. D., Twohy, C. H., Richardson, M., Eidhammer, T., and Rogers, D.: Predicting global atmospheric ice nuclei distributions and their impacts on climate, Proc. Natl. Acad. Sci., 107, 11217-11222, 2010.

Duft, D., and Leisner, T.: Laboratory evidence for volume-dominated nucleation of ice in supercooled water microdroplets, Atmos. Chem. Phys., 4, 1997-2000, 2004.

Fan, F., Zhang, S., Peng, Z., Chen, J., Su, M., Moghtaderi, B., and Doroodchi, E.: Numerical investigation of heterogeneous nucleation of water vapour on PM10 for particulate abatement, Can. J. Chem. Eng., 97, 930-939, 2019.

Fu, R., Hu, Y., Wright, J. S., Jiang, J. H., Dickinson, R. E., Chen, M., Filipiak, M., Read, W. G., Waters, J. W., and Wu, D. L.: Short circuit of water vapor and polluted air to the global stratosphere by convective transport over

the Tibetan Plateau, Proc. Natl. Acad. Sci., 103, 5664-5669, 2006.

Gao, B. C., Yang, P., Guo, G., Park, S. K., Wiscombe, W. J., and Chen, B.: Measurements of water vapor and high clouds over the Tibetan Plateau with the Terra MODIS instrument, IEEE Trans. Geosci. Remote Sens., 41, 895-900, 2003.

Gettelman, A., Liu, X., Ghan, S. J., Morrison, H., Park, S., Conley, A. J., Klein, S. A., Boyle, J., Mitchell, D. L., and Li, J. L.: Global simulations of ice nucleation and ice supersaturation with an improved cloud scheme in the Community Atmosphere Model, J. Geophy. Res. Atmos., 115, 2010.

Gryspeerdt, E., Sourdeval, O., Quaas, J., Delanoë, J., Krämer, M., and Kühne, P.: Ice crystal number concentration estimates from lidar-radar satellite remote sensing-Part 2: Controls on the ice crystal number concentration, Atmos. Chem. Phys., 18, 14351-14370, 2018.

Guignard, A., Stubenrauch, C., Baran, A., and Armante, R.: Bulk microphysical properties of semi transparent cirrus from AIRS: a six years global climatology and statistical analysis in synergy with CALIPSO and CloudSat, Atmos. Chem. Phys. Discuss., 11, doi:10.5194/acpd-11-24671-2011, 2011.

He, Q., Zheng, X., Li, J., Gao, W., Wang, Y., Cheng, T., Pu, J., Liu, J., and Li, C.: The role of ASM on the formation and properties of cirrus clouds over the Tibetan Plateau. Tellus, Ser. B: Chem. Phys. Meteorol., 71(1), 1577070.

Hendricks, J., Kärcher, B., and Lohmann, U.: Effects of ice nuclei on cirrus clouds in a global climate model, J. Geophys. Res. Atmos., 116, D18206, 2011.

Hoose, C. and Möhler, O.: Heterogeneous ice nucleation on atmospheric aerosols: a review of results from laboratory experiments, Atmos. Chem. Phys., 12, 9817–9854, 2012.

Hoose, C., and Möhler, O.: Heterogeneous ice nucleation on atmospheric aerosols: a review of results from laboratory experiments, Atmos. Chem. Phys., 12, 9817-9854, 2012.

Huang, J. P., Liu, Y. Z., Wang, T. H., Yan, H. R., Li, J. M., and He, Y. L.: An overview of the aerosol and cloud properties and water vapor budget over the Qinghai-Xizang Plateau, Plateau Meteor., 40, 1225-1240, 2021.

Jin, L. J., Yin, Y., Wang, P. X., and Chen, B. J.: Numerical modeling of tropical deep convective anvil and sensitivity test on its response to changes in the cloud condensation nuclei concentration, Chinese J. Atmos. Sci., 31, 793-804, 2007.

Kärcher, B. and Lohmann, U.: A parameterization of cirrus cloud formation: Heterogeneous freezing, J. Geophys. Res. Atmos., 108, doi:10.1029/2002JD003220, 2003.

Kay, J. E. and Wood, R.: Timescale analysis of aerosol sensitivity during homogeneous freezing and implications for upper tropospheric water vapor budgets, Geophys. Res. Lett., 35, L10809, 2008.

Khain, A., Ovtchinnikov, M., Pinsky, M., Pokrovsky, A., and Krugliak, H.: Notes on the state-of-the-art numerical modeling of cloud microphysics, Atmos. Res., 55, 159-224, 2000.

Khvorostyanov, V. I., Morrison, H., Curry, J. A., Baumgardner, D., and Lawson, P.: High supersaturation and modes of ice nucleation in thin tropopause cirrus: Simulation of the 13 July 2002 Cirrus Regional Study of Tropical Anvils and Cirrus Layers case, J. Geophys. Res. Atmos., 111, doi:10.1029/2004JD005235, 2006.

Kienast-Sjögren, E., Rolf, C., Seifert, P., Krieger, U. K., Luo, B. P., Krämer, M., and Peter, T.: Climatological and radiative properties of midlatitude cirrus clouds derived by automatic evaluation of lidar measurements, Atmos. Chem. Phys., 16, 7605-7621, 2016.

Kim, M. H., Omar, A. H., Tackett, J. L., Vaughan, M. A., Winker, D. M., Trepte, C. R., Hu, Y. X., Liu, Z. Y., Poole, L. R., Pitts, M. C., Kar, J., and Magill, B. E.: The CALIPSO version 4 automated aerosol classification and lidar ratio selection algorithm, Atmo. Meas. Tech., 11, 6107-6135, 2018.

Koop, T., and Murray, B.J.: A physically constrained classical description of the homogeneous nucleation of ice in water, J. Chem. Phys., 145, 211915-1-211915-11, 2016.

Ladino Moreno, L. A., Stetzer, O., and Lohmann, U.: Contact freezing: a review of experimental studies, Atmos. Chem. Phys., 13, 9745-9769, 2013.

Li, Q., Jiang, J. H., Wu, D. L., Read, W. G., Livesey, N. J., Waters, J. W., Zhang, Y., Wang, B., Filipiak, M. J., and Davis, C. P.: Convective outflow of South Asian pollution: A global CTM simulation compared with EOS MLS observations, Geophys. Res. Lett., 32, doi:10.1029/2005GL022765, 2005.

Liu, Z., Omar, A., Vaughan, M., Hair, J., Kittaka, C., Hu, Y. X., Powell, K., Trepte, C., Winker, D., Hostetler, C., Ferrare, R., and Pierce, R.: CALIPSO lidar observations of the optical properties of Saharan dust: A case study of long-range transport, J. Geophys. Res. Atmos., 113, doi: 10.1029/2007JD008878, 2008.

Lyu, K., Liu, X., and Kärcher, B.: Exploring sources of ice crystals in cirrus clouds: comparative analysis of two ice nucleation schemes in CAM6, Atmos. Chem. Phys., 25, 15369-15388, 2025.

Maeda, N.: Brief overview of ice nucleation. Molecules, 26, 392, 2021.

Mamouri, R. E., Ansmann, A., Ohneiser, K., Knopf, D. A., Nisantzi, A., Bühl, J., Engelmann, R., Skupin, A., Seifert, P., Baars, H., Ene, D., Wandinger, U., and Hadjimitsis, D.:Wildfire smoke triggers cirrus formation: lidar observations over the eastern Mediterranean, Atmos. Chem. Phys., 23, 14097-14114, 2023.

Mao, F., Shi, R., Rosenfeld, D., Pan, Z., Zang, L., Zhu, Y., and Lu, X.: Retrieving instantaneous extinction of aerosol undetected by the CALIPSO layer detection algorithm, Atmos. Chem. Phys., 22(16), 10589-10602, 2022.

McCluskey, C. S., DeMott, P. J., Prenni, A. J., Levin, E. J., McMeeking, G. R., Sullivan, A. P., Hill, T. C., Nakao, S., Carrico, C. M., and Kreidenweis, S. M.: Characteristics of atmospheric ice nucleating particles associated with biomass burning in the US: Prescribed burns and wildfires, J. Geophys. Res. Atmos., 119, 10458-10470, 2014.

Morris, C. E., Georgakopoulos, D. G., and Sands, D. C.: Ice nucleation active bacteria and their potential role in precipitation, J. Phys. IV France., 121,87-103, 2004.

Murray, B. J., Broadley, S. L., Wilson, T. W., Bull, S. J., Wills, R. H., Christenson, H. K., Murray, E. J.: Kinetics of the homogeneous freezing of water, Phys. Chem. Chem. Phys., 12, 10380–10387, 2010.

Murray, B. J., O'sullivan, D., Atkinson, J. D., and Webb, M. E.: Ice nucleation by particles immersed in supercooled cloud droplets, Chem. Soc. Rev., 41, 6519-6554, 2012.

Murray, B. J., Wilson, T. W., Dobbie, S., Cui, Z., Al-Jumur, S. M., Möhler, O., Schnaiter, M., Wagner, R., Benz, S., and Niemand, M.: Heterogeneous nucleation of ice particles on glassy aerosols under cirrus conditions, Nat. Geosci., 3, 233-237, 2010.

Prabhakara, C., Kratz, D., Yoo, J.-M., Dalu, G., and Vernekar, A.: Optically thin cirrus clouds: Radiative impact on the warm pool, J. Quant. Spectrosc. Radiat. Transfer., 49, 467-483, 1993.

Prenni, A. J., DeMott, P. J., Sullivan, A. P., Sullivan, R. C., Kreidenweis, S. M., and Rogers, D. C.: Biomass burning as a potential source for atmospheric ice nuclei: Western wildfires and prescribed burns, Geophy. Res. Lett., 39, L11805, 2012.

Randel, W. J., Park, M., Emmons, L., Kinnison, D., Bernath, P., Walker, K. A., Boone, C., and Pumphrey, H.: Asian monsoon transport of pollution to the stratosphere, Science, 328, 611-613, 2010.

Shi, X. J., Zhu, S. P., Zhi, X. F., Du, K. Y., Liu, Q. G., and Wang, L. W.:Sensitivity study on three ice nucleation parameterizations, Trans. Atmos. Sci., 40, 181-192, 2017.

Shi, X., Liu, X., and Zhang, K.: Effects of pre-existing ice crystals on cirrus clouds and comparison between different ice nucleation parameterizations with the Community Atmosphere Model (CAM5), Atmos. Chem. Phys., 15, 1503-1520, 2015.

Sourdeval, O., Gryspeerdt, E., Krämer, M., Goren, T., Delanoë, J., Afchine, A., Hemmer, F., and Quaas, J.: Ice crystal number concentration estimates from lidar-radar satellite remote sensing-Part 1: Method and evaluation, Atmos. Chem. Phys., 18, 14327-14350, 2018.

Stephens, G. L.: Cloud feedbacks in the climate system: A critical review, J. Climate., 18, 237-273, 2005.

Sun, N., Fu, Y., Zhong, L., Zhao, C., & Li, R.: The impact of convective overshooting on the thermal structure over the Tibetan Plateau in summer based on TRMM, COSMIC, Radiosonde, and Reanalysis Data. J. Climate, 34, 8047-8063, 2021.

Takahashi, H. and Luo, Z.: Where is the level of neutral buoyancy for deep convection? Geophys. Res. Lett., 39, 2012.

Wang, C. M., Ye, J. D. and Wei, S. Y.: A numerical experiment of aerosol concentration affecting warm rain process, Scientia Meteor. Sinica, 17, 316-323, 1997.

Wang, H. Q., and Zhao, G. X.: Cloud and Radiation-I: Cloud climatology and radiative effects of clouds, Scientia Atmos. Sinica, 18, 910-932, 1994.

Wang, K., Chen, J., Hong, Z. C., Yan, C. Q., and He, Q. S.: Research of the distribution characteristics and generation mechanism of cirrus clouds over the Qinghai-Xizang Plateau in summer, Plateau Meteor., doi:10.7522/j. issn. 1000-0534. 2022. 00069, 2023.

Wang, P. H., Minnis, P., McCormick, M. P., Kent, G. S., and Skeens, K. M.: A 6-year climatology of cloud occurrence frequency from Stratospheric Aerosol and Gas Experiment II observations (1985-1990), J. Geophys. Res. Atmos., 101, 29407-29429, 1996.

Xie, S. F., Wang, Y. J., Huang, L. K., Pan, Q. Y., and Wei, P. Z.: Accuracy analysis of Tm calculated by ERA5 and MERRA-2 reanalysis data over China, J. Geo. Geodyn., 41, 771-776, 2021.

Xue, X. N, Deng, X. B., and Liu, G. H.: Study on characteristics of Qinghai-Tibetan Plateau cirrus based on satellite data, Plateau Meteor., 37, 505-513, 2018.

Yang, Y. K., Zhao, C. F., and Fan, H.: Spatiotemporal distributions of cloud properties over China based on Himawari-8 advanced Himawari imager data, Atmos. Res., 240, doi:10.1016/j.atmosres.2020.104927, 2020.

Zhang, F., Yu, Q. R., Mao, J. L., Dan, C., Wang, Y., He, Q., Cheng, T., Chen, C., Liu, D., and Gao, Y.: Possible mechanisms of summer cirrus clouds over the Tibetan Plateau, Atmos. Chem. Phys., 20, 11799-11808, 2020.

Zhang, K., Liu, X., Wang, M., Comstock, J. M., Mitchell, D. L., Mishra, S., and Mace, G. G.: Evaluating and constraining ice cloud parameterizations in CAM5 using aircraft measurements from the SPARTICUS campaign, Atmos. Chem. Phys., 13, 4963-4982, 2013.

Zhao, B., Liou, K. N., Gu, Y., Jiang, J. H., Li, Q., Fu, R., Huang, L., Liu, X., Shi, X., Su, H., and He, C.: Impact of aerosols on ice crystal size, Atmos. Chem. Phys., 18, 1065-1078, 2018.

Zhao, C., Chen, Y., Li, J., Letu, H., Su, Y., Chen, T., and Wu, X.: Fifteen-year statistical analysis of cloud characteristics over China using Terra and Aqua Moderate Resolution Imaging Spectroradiometer observations, Int. J. Climatol., 39, 2612-2629, 2019.

Zheng, J. Y., Liu, D., Wang, Z. E., Tian, X. M., Wang, Y. J., and Xie, C. B.: Global distribution and seasonal variation of clouds observed from CloudSat/CALIPSO, Acta Meteor. Sinica., 76, 420-433, 2018.

删除[凯']: Austin, R. T., Heymsfield, A. J., and Stephens, G. L.: Retrieval of ice cloud microphysical parameters using the CloudSat millimeter-wave radar and temperature, J. Geophys. Res., 114, doi:10.1029/2008JD010049, 2009.

Austin, R. T.: Level 2B radar-only cloud water content (2B-CWC-RO) process description document, Data Processing Center, 24, 2007.

Barahona, D. and Nenes, A.: Parameterizing the competition between homogeneous and heterogeneous freezing in ice cloud formation-polydisperse ice nuclei, Atmos. Chem. Phys., 9, 5933-5948, 2009.

Baran, A. J.: From the single-scattering properties of ice crystals to climate prediction: A way forward, Atmos. Res., 112, 45-69, 2012.

Cairo, F., Krämer, M., Afchine, A., Di Donfrancesco, G., Di Liberto, L., Khaykin, S., Lucaferri, L., Mitev, V., Port, M., Rolf, C., Snels, M., Spelten, N., Weigel, R., and Borrmann, S.: A comparative analysis of in situ measurements of high-altitude cirrus in the tropics, Atmos. Meas. Tech., 16, 4899-4925, 2023.

Cantrell, W. and Heymsfield, A.: Production of ice in tropospheric clouds: A review, Bull. Am. Meteorol. Soc., 86, 795-808, 2005.

Chen, B. and Liu, X.: Seasonal migration of cirrus clouds over the Asian Monsoon regions and the Tibetan Plateau measured from MODIS/Terra, Geophys. Res. Lett., 32, doi:1029/2004GL020868, 2005.

Chen, Q. L., Gao, G. L., Li ,Y., Cai, H. K., Zhou, X., and Wang, Z. L.: Main detrainment height of deep convection systems over the Tibetan Plateau and its southern slope, Adv. Atmos. Sci., 36, 1078-1088, 2019.

Chen, Y., DeMott, P. J., Kreidenweis, S. M., Rogers, D. C., and Sherman, D. E.: Ice formation by sulfate and sulfuric acid aerosol particles under upper-tropospheric conditions, J. Atmos. Sci., 57, 3752-3766, 2000.

Comstock, J. M., Lin, R. F., Starr, D. O. C., and Yang, P.: Understanding ice supersaturation, particle growth, and number concentration in cirrus clouds, J. Geophys. Res. Atmos., 113, D23211, 2008.

Delanoë, J., and Hogan, R. J.: A variational scheme for retrieving ice cloud properties from combined radar, lidar, and infrared radiometer, J. Geophys. Res., 113, D07204, 2008.

Delanoë, J., and Hogan, R. J.: Combined CloudSat-CALIPSO-MODIS retrievals of the properties of ice clouds, J. Geophys. Res., 115, D00H29, 2010.

DeMott, P. J., Prenni, A. J., Liu, X., Kreidenweis, S. M., Petters, M. D., Twohy, C. H., Richardson, M., Eidhammer, T., and Rogers, D.: Predicting global atmospheric ice nuclei distributions and their impacts on climate, Proc. Natl. Acad. Sci., 107, 11217-11222, 2010.

Fan, F., Zhang, S., Peng, Z., Chen, J., Su, M., Moghtaderi, B., and Doroodchi, E.: Numerical investigation of heterogeneous nucleation of water vapour on PM10 for particulate abatement,